A picosecond holographic grating approach to molecular dynamics in oriented liquid crystal films

Gregory Eyring and M. D. Fayer
Department of Chemistry, Stanford University, Stanford, California 94305

(Received 26 April 1984; accepted 16 July 1984)

The picosecond transient grating technique offers a new approach to the characterization of rotational dynamics and mechanical properties of thin liquid crystal films. Sample excitation by two crossed 100 ps pulses having parallel polarization results in two kinds of phase gratings: one due to the optical Kerr effect, and the other to a standing longitudinal acoustic wave. Rotational reorientation times are calculated from the relaxation of the Kerr grating, while the ultrasonic velocity and absorption are obtained by monitoring the acoustic response. If the excitation pulses are perpendicularly polarized, no longitudinal acoustic waves are generated, so that the signal is due exclusively to the Kerr effect. Whereas previous workers using ~20 ns excitation pulses observed a single exponential Kerr relaxation in the isotropic phase, we are able to resolve the decay into a fast nonexponential component followed by a slow exponential component. While the slow component disappears below the isotropic→nematic transition, we can detect the fast component even below the nematic→smectic A transition in CBOA. An explanation of the fast component is proposed involving individual rather than collective molecular reorientation. The nature of the polarization grating resulting from perpendicularly polarized excitation pulses is described. An unusual property of this grating is that it acts like a half-wave plate for the diffracted signal. Thus the polarizations of the incoming probe and the outgoing diffracted pulses can be made orthogonal. The theory and implications of this result are discussed, and the extension of the transient grating technique to the study of model biological membranes is outlined.

INTRODUCTION

The transient grating technique has been used to study a wide variety of molecular dynamic phenomena[1] including energy transport,[2] molecular rotation,[3] and acoustic wave propagation in bulk liquids and solids.[4,5] Here we demonstrate that this technique can be readily extended to explore rotational dynamics and mechanical properties of thin films of oriented liquid crystals. Due in part to the importance of these properties to the technological applications of liquid crystals, they have been the object of intense research in the past decade. Two of the most useful probes in these experiments have been the optical Kerr effect[6–8] and ultrasonic wave propagation.[9] In the former case, the linear birefringence induced by an intense excitation laser pulse causes a rotation of the polarization of a weaker probe beam which decays with the rotational reorientation time of the molecules; in the latter, the phase velocity and attenuation of acoustic waves provide information about the elasticity and viscosity of the various phases, as well as about the critical phenomena associated with the phase transitions. Using a transient grating, both the optical Kerr effect and ultrasonic wave propagation can be observed in the same experiment. We will show that the optical Kerr response can be conveniently isolated from the acoustic response by manipulating the relative polarizations of the excitation pulses.

Briefly, the typical experiment proceeds as follows. Samples are exposed to two crossed, picosecond excitation pulses having the same wavelength and polarization. Constructive and destructive interference in the crossing volume produces a sinusoidally varying pattern of intensity peaks and nulls which stimulates both Kerr and acoustic responses in the sample. This results in a periodic modulation of the refractive index, which acts as a diffraction grating for a variably delayed probe pulse. The changes in diffracted probe intensity as a function of time following the grating excitation reflect dynamical processes within the sample.

The versatility of the transient grating technique arises from the multiplicity of ways in which intense laser fields can alter the refractive index of materials.[1] These may be classed into two categories, depending on whether they involve changes in the real or imaginary part of the complex refractive index $\tilde{n}$:

$$\tilde{n} = n + ik. \tag{1}$$

In general, the diffracted probe intensity is a superposition of diffraction from both phase (real part) and amplitude (imaginary part) gratings. However, effects due to amplitude gratings are important only when both the excitation and probe wavelengths lie within allowed electronic absorption bands of the sample. In the work described here both the excitation (1.06 μ) and probe (532 nm) lie well to the red of the liquid crystal singlet absorption (<400 nm). Therefore, all amplitude grating effects are negligible.

We have found that there are two contributions to the phase grating diffraction in liquid crystal films. The first is due to periodic variations in the density associated with the propagation of a standing acoustic wave which has the same wavelength and wave vector as the grating. The time dependence of the peak–null difference in refractive index has been shown to be

 0021-9606/84/224314-08$02.10

$$\Delta n^{ac}(t) \propto \{A\,[1-\cos\omega t\cdot\exp(-\alpha Vt)]$$

$$-B\,[\sin\omega t\cdot\exp(-\alpha Vt)]\}, \quad (2)$$

where ω is the circular frequency of the acoustic wave, V is its phase velocity, and α is its attenuation constant (cm^{-1}). The first term in Eq. (2) describes acoustic waves generated by the impulsive heating in the intensity peaks, while the second accounts for waves launched by electrostrictive perturbations of the density caused by the large optical field. Thus, the constants A and B depend on the absorption cross section and the opto-elastic constant, respectively.[5]

The second contribution to the phase grating diffraction is from the optical Kerr effect. This also has two components: an electronic part and an orientational part. The optical field can distort the electron cloud through its interaction with the electronic hyperpolarizability.[6] The probe then experiences a peak–null change in the refractive index given by[8]

$$\Delta n^{e}(t) = \frac{n_2^e}{\tau_e}\int_{-\infty}^{t} E^2(t')\exp\left(-\frac{(t-t')}{\tau_e}\right)dt', \quad (3)$$

where n_2^e is proportional to a sum of elements of the fourth rank hyperpolarizability tensor, τ_e is the electronic relaxation time ($\sim 10^{-15}$ s), and $E(t)$ is the instantaneous optical field strength. An additional Kerr effect which is important in liquid crystals involves laser-induced molecular orientation arising from interaction between the optical field and the polarizability anisotropy of the molecules. In this case the peak–null change in index due to molecular orientation is[8]

$$\Delta n^{0}(t) = \frac{n_2^0}{\tau_0}\int_{-\infty}^{t} \bar{E}^2(t')\exp\left(-\frac{(t-t')}{\tau_0}\right)dt', \quad (4)$$

where n_2^0 is a measure of the anisotropy of the molecular polarizability, $\bar{E}^2(t')$ is the rms electric field strength at a given point in the grating, and τ_0 is the rotational reorientation time (10^{-10}–10^{-6} s). It is implicitly assumed in Eq. (4) that the rotational diffusion is adequately characterized by a single time τ_0.

In a liquid crystal transient grating experiment using excitation pulses of parallel polarization, both the acoustic and Kerr effects contribute to the intensity of probe diffraction:

$$I(t) \propto [\Delta n^{ac}(t) + \Delta n^{e}(t) + \Delta n^{0}(t)]^2. \quad (5)$$

Because the electronic cloud relaxation time τ_e (10^{-15} s)[6] is so short relative to the pulse duration ($\sim 10^{-10}$ s), Δn^e contributes only during the period when the excitation and probe pulses are simultaneously present in the sample. However, the orientational relaxation time τ_0 may range up to several hundred nanoseconds,[6] and depends strongly on the proximity to the isotropic→nematic phase transition. Thus, after parallel-polarized excitation pulses have passed through the sample, the phase grating induced in the liquid crystal film is a superposition of standing acoustic wave and orientational Kerr effects.

It is possible to separate out these two responses by rotating the polarization of one excitation pulse so that it is exactly perpendicular to the other. In this configuration the optical fields in the two pulses do not interfere, so that the intensity in the crossing volume varies smoothly as the Gaussian transverse mode of the laser. Without the sinusoidal intensity modulation, no longitudinal acoustic waves are generated.[10] Nevertheless, while the optical fields cannot constructively and destructively interfere, they still add together vectorially to produce a periodic variation in the net polarization.[11] This gives rise to a "polarization grating" having the identical wavelength and direction as the intensity grating discussed above. The liquid crystal molecules respond to the polarization grating through the orientational Kerr effect. Thus, the use of perpendicularly polarized excitation pulses permits the rotational dynamics of the liquid crystals to be analyzed in the absence of complications due to the acoustic response.

In this paper we analyze the transient grating signal from $\sim 280\,\mu$m thick films of the liquid crystals *p*-*n*-pentyl-*p'*-cyanobiphenyl (5CB) and *N*-(*p*-cyanobenzylidene-*p*-octyloxyaniline) (CBOA) for both parallel and perpendicular excitation pulse polarizations. Representative data are shown for the isotropic, nematic, and (in CBOA) the smectic A phase from which the acoustic velocity and attenuation, as well as the rotational reorientation times, are computed. We observe a fast nonexponential component to the Kerr relaxation in all of the phases which was not resolved by previous workers who used ~ 20 ns laser pulses.[6] This fast decay is interpreted as the time required for individual molecules to undergo restricted rotational diffusion in the potential "cage" formed by their near neighbors.

Finally, a useful aspect of the polarization grating is that the diffracted signal has a polarization which is rotated up to 90° relative to the transmitted probe polarization. In other words, the perpendicularly polarized excitation pulses generate a transient half-wave plate for the diffracted probe wave. The theory and implications of this result for enhancing transient grating experiments will be discussed.

EXPERIMENTAL PROCEDURES

The laser system used in these experiments has been described in detail previously.[1] A continuously pumped Nd:YAG oscillator is acousto-optically mode-locked and *Q*-switched to produce 1.06 μm pulses at 400 Hz. The output is a train of some 40 mode-locked pulses of width ~ 100 ps and separated by 9 ns. A $\sim 50\,\mu$J pulse from the center of the train is selected out by a Pockels cell. A small portion of the Ir single pulse is frequency doubled using CD*A to give a $\sim 5\,\mu$J probe at 532 nm. The remainder is beamsplit to give two $\sim 15\,\mu$J pulses which, after traveling equal path lengths, are crossed at an angle θ in the sample (Fig. 1). The sample is thus exposed to a sinusoidally varying pattern of intensity peaks and nulls produced by the interference between the IR excitation beams. The fringe spacing is given by

$$\Lambda = \frac{\lambda}{2\sin(\theta/2)}, \quad (6)$$

where λ is the laser wavelength. In this work, Λ was kept constant at $\sim 3.9\,\mu$m.

The interaction region of the IR excitation beams is probed at the Bragg angle with 532 nm pulse which could be

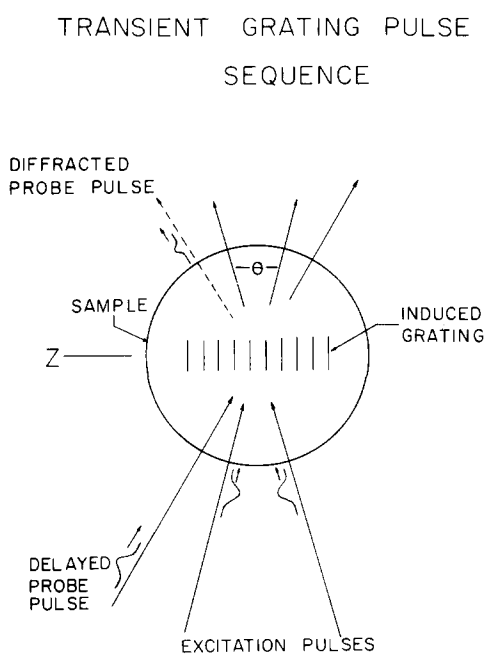

FIG. 1. Schematic illustration of the transient grating experiment. The crossed excitation pulses generate periodic Kerr effect alignment and a standing acoustic wave in the liquid crystal film having the wavelength and orientation (wave vector along Z) of the optical interference pattern. The resulting changes in the index of refraction create a diffraction grating which Bragg diffracts a delayed probe pulse. If the excitation pulses are perpendicularly polarized, the diffracted probe signal comes from the Kerr grating only, and its polarization may be rotated by 90° relative to the incident probe polarization.

timed to arrive continuously from 1 ns before to 16 ns after the IR excitation, using an optical delay line. Spot sizes of the excitation and probe beams were 100 and 60 μm, respectively. Under these conditions, the rms electric field at the peak of the excitation pulse is about 10^6 volt/cm. The probe diffraction was detected with a photodiode coupled to a lock-in amplifier, and signal from each scan of the optical delay line was stored on a computer for subsequent analysis.

The liquid crystals CBOA (Eastman, $I \rightarrow N = 107°$; $N \rightarrow S = 83°$) and 5CB (BDH, $I \rightarrow N = 35°$) were filtered through a pore size of 0.1 μm to remove dust particles. This was necessary to avoid complications due to bubble gratings.[12] They were then sandwiched between fused silica optical flats using a Teflon spacer of 125 or 280 μm thickness. The surface of the flats had been treated with octadecyltrichlorosilane (Petrarch Systems) which is known to produce homeotropic alignment (director perpendicular to the surface) of nematic liquid crystal films. The alignment could be readily verified by the characteristic dark cross in the conoscopic pattern under a polarizing microscope. This assembly was inserted into a variable temperature cell which could be heated resistively up to 200 °C. The temperature was monitored using a 3 mm platinum resistance thermometer (Omega, GSO 330) which was inserted into a hole drilled into one of the optical flats. The temperature was constant to $\pm$ 0.2 °C. In a typical experiment, the temperature was raised above the nematic→isotropic transition and the sample was cooled slowly to yield the homeotropically aligned nematic and (in the case of CBOA) smectic A phases. The degree of alignment was independent of whether the 125 or 280 μm spacer was used.

RESULTS AND DISCUSSION

Typical results of a transient grating experiment on the isotropic phase of 5CB at 42 °C are shown in Fig. 2, where diffracted probe intensity is plotted as a function of probe delay time. The signal rises to a maximum at $t = 0$ when the excitation and probe pulses are simultaneously inside the sample, due to the electronic Kerr effect. Diffracted intensity then falls off rapidly with the cross correlation time of the excitation and probe pulses until it reaches a value determined by the amplitude of the orientational Kerr effect. The signal then decays more slowly with the molecular reorientation time. For parallel-polarized excitation pulses (Fig. 2A), this decay is modulated by diffraction from a standing acoustic wave generated by the intensity grating. In order to simplify the discussion, we will assume that the acoustic wave is generated exclusively by the electrostriction mechanism. Equation (2) then simplifies to[4]

$$\Delta n^{ac}(t) \propto B \sin \omega t \cdot \exp(-\alpha V t). \tag{7}$$

Using Eqs. (4), (5), and (7), if we consider the signal at times long compared to the pulse duration we can neglect $\Delta n^e(t)$ to obtain

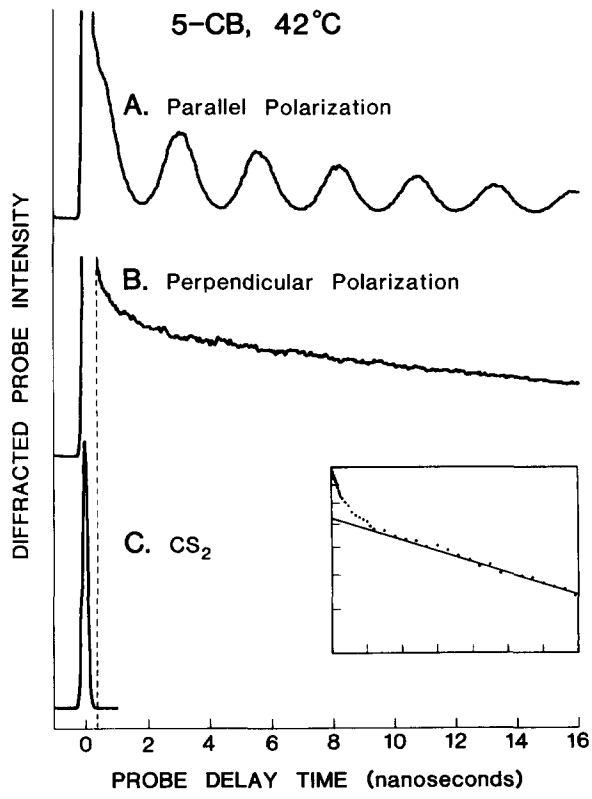

FIG. 2. The diffracted probe intensity as a function of probe delay time in the isotropic phase of 5CB at 42 °C for the case of parallel (A) and perpendicular (B) polarized excitation pulses. Also shown for comparison in C is the signal from CS_2, which gives the cross correlation of the excitation and probe pulses. Inset in B is a semilogarithmic plot of the data starting at $t = 400$ ps (dotted line). The inset horizontal scale is 2 ns per division.

$$I(t) \propto [K \exp(-t/\tau_0) - B \sin \omega t \cdot \exp(-\alpha V t)]^2 \quad (8a)$$

$$= K^2 \exp(-2t/\tau_0) - 2KB \sin \omega t \cdot \exp(-\alpha V t) \exp(-t/\tau_0) + B^2 \sin^2 \omega t \cdot \exp(-2\alpha V t), \quad (8b)$$

where $K \propto n_2^0/\tau_0$.

The latter two terms in Eq. (8b) are responsible for the periodic modulation of the signal in Fig. 2A.

The signal obtained using a perpendicularly polarized excitation pulses is shown in Fig. 2B. As noted above, under these conditions no longitudinal acoustic waves are generated since $n_{\text{peak}}^{\text{ac}} = n_{\text{null}}^{\text{ac}}$, and according to Eq. (8b) the diffraction should decay exponentially as $\exp(-2t/\tau_0)$. The inset is a semilogarithmic plot of the data starting at $t_d = 400$ ps. At long times the plot is linear, but at short times there is a marked deviation from linearity. We verified that this deviation is not due to pulse convolution effects as follows. The transient grating signal is the convolution of the Gaussian probe pulse $I_p(t)$ with $\Delta n^0(t)^2$. We have for the diffracted intensity as a function of delay time t_d:

$$I(t_d) = \Delta n^0(t)^2 * I_p(t) = \int_{-\infty}^{\infty} dt\, \Delta n^0(t)^2 I_p(t - t_d). \quad (9)$$

From Eq. (4) we see that $\Delta n^0(t)$ is itself a convolution of the Gaussian excitation pulse with the impulse response function, assumed to be a single exponential, $\exp(-t/\tau_0)$. We performed a series of numerical calculations involving a double convolution of two Gaussians of ~ 100 ps FWHM with an exponential having a 50 ns lifetime. In each case we found that for times longer than twice the FWHM of the cross correlation of the two Gaussians, the convolution effects were negligible, i.e., the decay was perfectly exponential. We obtained the cross correlation of our excitation and probe pulses from the transient grating signal in CS_2. CS_2 is known to have a 2 ps rotational correlation time at room temperature,[13] and thus has a delta function impulse response for our 100 ps pulses. The CS_2 signal is shown in Fig. 2B and has a FWHM of ~ 140 ps. Therefore, for delay times longer than 400 ps after $t_d = 0$, we can be sure that the diffracted signal is due only to the impulse response of the liquid crystal films.

The inset in Fig. 2B shows clearly that the assumption of a single exponential decay for the orientational Kerr effect is not valid. Moreover, the fast component is nonexponential, and is itself composed of a range of decay times from ~ 200 ps to 2 ns. Previous optical Kerr studies[6,7] in the isotropic phase of nematic liquid crystals used ~ 20 ns excitation pulses, and were not able to resolve this fast component. They did, however, obtain accurate values of τ_0, the order parameter relaxation time, which is associated with collective rotation about the short axis of the molecules. A fit of the exponential tail of the data in Fig. 2B yields τ_0, the order parameter relaxation time, which is associated with collective rotation about the short axis of the molecule. We obtain $\tau_0 = 53 \pm 8$ ns, which is consistent with the previously measured value of $\tau_0 = 60$ ns in 5CB at 42 °C.[7] The uncertainty in τ_0 arises from the fact that our optical delay line only allows us to follow the decay out to ~ 16 ns, much less than one lifetime. A more precise value could be obtained using a cw probe or a longer delay line.

Several theories have been proposed which predict a fast and a slow component to the Kerr relaxation in concentrated solutions of rodlike molecules.[14–16] The fast component is associated with relatively free rotational diffusion of a rod within a tube formed by the near neighbors, while the slow component is due to small step rotational diffusion of the tube axis. Several light scattering and dielectric relaxation studies on semidilute solutions of rigid rod macromolecules appear to confirm the presence of two relaxation time scales.[16] However, a recent review of dielectric relaxation studies of neat liquid crystals does not report an absorption in the 10^{-10}–10^{-9} s range.[17] Nevertheless, we can be certain that the fast component is due to rotation about the short molecular axis, since rotation about the long axis does not change the index of refraction.

In Fig. 2A the (circular) acoustic frequency $\omega = 2.46$ GHz is readily found from the spacing τ between the peaks in the diffraction:

$$\omega = 2\pi/\tau \quad (10)$$

and the acoustic velocity $V = 1.54 \times 10^5$ cm/s is obtained from

$$V = \frac{\Lambda \omega}{2\pi}, \quad (11)$$

where $\Lambda = 3.95\,\mu$m is the acoustic wavelength defined in Eq. (6). Since at frequencies f higher than ~ 50 MHz the attenuation is proportional to f^2, the quantity α/f^2 is usually reported to facilitate comparison of attenuations measured at different frequencies. Knowing the value of τ_0 from Fig. 2B we can estimate the value of $\alpha/f^2 = 330 \pm 150 \times 10^{-17}$ s^2/cm, which agrees within our uncertainty with the value of $\sim 500 \times 10^{-17}$ s^2/cm measured at 100 MHz, using more conventional transducer techniques.[18]

The nature of the gratings produced in the cases of parallel and perpendicular-polarized excitation pulses is shown in Fig. 3. Depicted are the variations of the electric field in a plane perpendicular to the bisector of the angle between the excitation beams, together with the resulting Kerr effect alignment of the liquid crystal molecules. In the parallel case, the continuous change in relative phase Φ of the two excitation beam wave fronts results in a sinusoidal pattern of constructive and destructive interference such that if E is the field strength in one excitation beam, the field in the grating peaks is $2E$, and 0 in the nulls. From Eq. (4), the optically induced Kerr orientation in the peaks is proportional to $(2\bar{E})^2 = 4\bar{E}^2$. The degree of induced alignment varies as the intensity across the grating.

An important point here is that because the excitation pulses have parallel polarization, the changes in relative phase of the two wave fronts result in a variation of the amplitude, but not of the linearly polarized nature of the net field. This is not the case for perpendicularly polarized excitation pulses, as shown in Fig. 3B. Here the changes in relative phase cause the polarization of the net field to vary from linear to elliptical to circular and back.[11] Note that for phase differences of 0 and π, the net polarizations are linear but

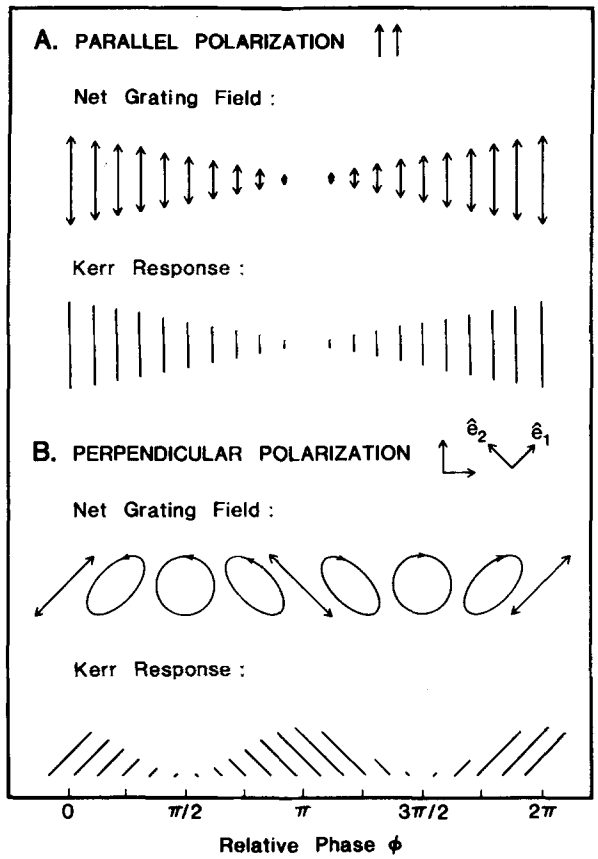

FIG. 3. The variation of the grating electric field and resulting molecular alignment as a function of the relative phase angle ϕ between the excitation pulses for parallel (A) and perpendicular (B) polarization. A is an intensity grating which results in a superposition of the Kerr effect and an acoustic standing wave of wavelength Λ. B is a polarization grating in which the field varies between linear, elliptical, and circular polarization. Since the overall intensity in B remains constant, there is no acoustic response, and only the Kerr effect contributes to the probe diffraction. The length of the bars is proportional to the degree of induced orientation. The two orientation directions in B are labeled $\hat{e}_1$ and $\hat{e}_2$.

orthogonal. We designate these two directions $\hat{e}_1$ and $\hat{e}_2$. The fringe spacing Λ in Fig. 3A corresponds to a phase variation of 2π in Fig. 3B.

In order to understand the response of the liquid crystal molecules to the grating in Fig. 3B, we note that an elliptically polarized field can always be described as the superposition of a linearly and a circularly polarized field. Since a circularly polarized field is just two perpendicularly polarized linear components with phase difference $\pi/2$, it cannot produce any net alignment of molecules through the optical Kerr effect. Thus, in the regions of pure circular polarization at $\phi = \pi/2$, $3\pi/2$, etc., the refractive index retains its isotropic value. Conversely, the maximum excursions of the refractive index occur in the regions of pure linear polarization at $\phi = 0$, π, 2π, etc. Again taking the amplitude of the field in each excitation beam to be E, the linearly polarized field amplitude $E_l = \sqrt{2}E$ at $\phi = 0$, π, 2π... and $E_l = 0$ at $\phi = \pi/2$, $3\pi/2$, $5\pi/2$.... The induced peak Kerr orientation is $(\sqrt{2}\bar{E})^2 = 2\bar{E}^2$. Thus we can see that, in contrast to Fig. 3A, in which the degree of alignment varies as the grating intensity, in Fig. 3B it varies not with the overall intensity, but with the intensity of the linearly polarized component. This intensity variation is a factor of 2 smaller than in Fig. 3A.

Up to this point we have not discussed how the magnitude K of the optical Kerr grating depends on the physical state of the liquid crystals. Figure 4 shows typical relaxation curves for CBOA in the isotropic (A), nematic (B), and smectic A (C) phases using perpendicularly polarized excitation pulses. Curves B and C have been blown up by a factor of 10 and 100 compared with A, respectively.

Qualitatively, the amplitude of the long component of the Kerr relaxation is large in the isotropic phase and disappears in the nematic and smectic A phases. A fit of the tail in Fig. 2A yields $\tau_0 = 60 \pm 20$ ns. The fast relaxation is still measurable in the nematic and smectic A, although its amplitude is reduced by a factor of 10 in B, and another factor of 3 in C, relative to A. The disappearance of the τ_0 relaxation at the $I \rightarrow N$ transition can be understood in terms of the onset of the "nematic barrier."[19] With homeotropic orientation, our net grating field is everywhere perpendicular to the director. In order to align themselves with the field, the molecules must overcome this barrier. The torques generated by our 100 ps pulses are not sufficient to produce the collective rotation associated with τ_0. Such "optical Freedericz transitions" are, however, readily seen with relatively low power cw lasers.[20] The fact that the fast relaxation is observed below the $I \rightarrow N$ transition argues that it is associated with indi-

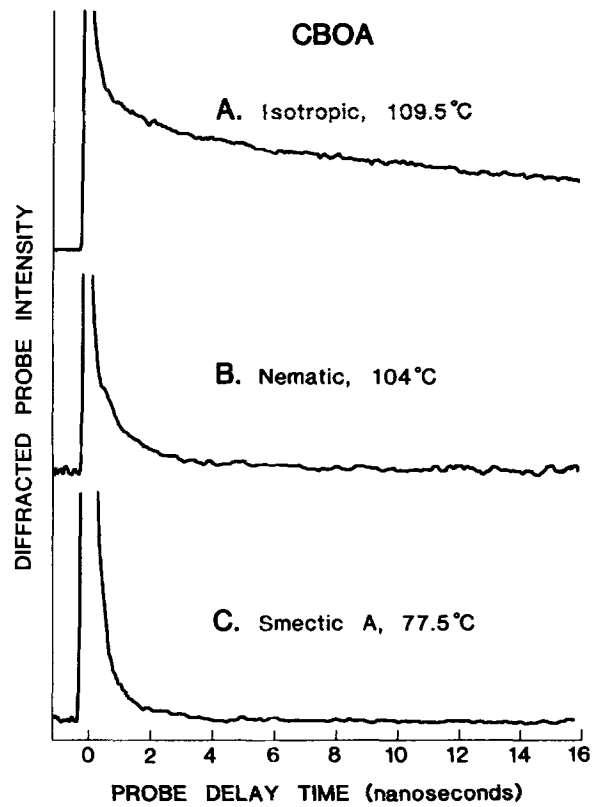

FIG. 4. Diffracted probe intensity as a function of probe delay time in the isotropic (A), homeotropically aligned nematic (B), and smectic A (C) phases of CBOA for perpendicularly polarized excitation pulses. The vertical scales in B and C are expanded by factors of 10 and 100 relative to A. In the isotropic phase the orientational Kerr relaxation is characterized by a relatively slow exponential component and a distribution of fast components. Only the fast components are observed below $I \rightarrow N$ transition.

vidual rather than collective rotational reorientation. We envision that, due to statistical fluctuations of the molecular long axes about the director, random "pockets" develop into which molecules can be rotated by the optical field. The relaxation occurs over a range of times which depend on the initial pocket characteristics. The decreasing apparent amplitude of the fast component with decreasing temperature may in fact be a shift in the distribution of relaxation times toward shorter time; this is expected since the size of the pockets is reduced as the order parameter increases. Due to the small relative amplitude of the effect as well as the distribution of relaxation times, it is doubtful that it could be observed in a dielectric relaxation experiment. This illustrates the advantage of the direct time-domain measurement afforded by the picosecond transient grating technique. Due to limitations imposed by the pulse durations used in these experiments, it was not possible to observe the full range of relaxation times postulated above. Experiments on a 1 ps time scale would provide a test of the proposed model.

Figure 5 displays the same data as Fig. 4, but with parallel rather than perpendicularly polarized excitation pulses. The signal here is a superposition of the orientational Kerr effect and the acoustic effect as described in Eq. (8). In the isotropic phase (Fig. 5A), 2.5 °C above the $I \rightarrow N$ transition, $K \gg B$ and the amplitude of the acoustic modulation is given by the cross term. Note that because $K^2 > 2KB$ the signal "nulls" do not reach the base line. We obtain $\omega = 2.25$ GHz and $V = 1.36 \times 10^5$ cm/s at this temperature. Knowing τ_0 we can estimate the acoustic damping parameter $\alpha/f^2 = 250 \times 10^{-17}$ s^2/cm which is consistent with values measured previously.[18] Just below the $I \rightarrow N$ transition in Fig. 5B the fast components of the Kerr decay still contribute and the diffraction peaks actually get larger with increasing delay time. This can only happen if the acoustic term is larger than the Kerr term and the two are added with opposite sign in Eq. (8). Physically, this means that the refractive index changes in the intensity peaks due to the Kerr and acoustic responses have opposite signs. From the acoustic period we obtain $\omega = 2.27$ GHz and $V = 1.38 \times 10^5$ cm/s in the nematic phase at this temperature. Finally, in Fig. 5C, 5 °C below the $N \rightarrow S_A$ transition, the acoustic term dominates, with two unequal diffraction peaks per acoustic cycle. This pattern is characteristic of a superposition of electrostrictively and thermally generated acoustic waves.[5] Our neglect of the heating mechanism [first term in Eq. (2)] was therefore an oversimplification. The heating is due to weak absorption of the IR excitation pulses into the forbidden $v = 0 \rightarrow v = 3$ transition of C–H stretching modes, followed by rapid radiationless relaxation. We estimate that the intensity peaks are heated by no more than 10^{-3} K per shot. A fit to the data in Fig. 5C obtains $\omega = 2.46$ GHz, $V = 1.49 \times 10^5$ cm/s, and $\alpha/f^2 = 300 \pm 100 \times 10^{-17}$ s^2/cm; as compared with the value of $\alpha/f^2 = 158 \times 10^{-17}$ s^2/cm measured previously at 560 MHz.[18]

The foregoing demonstrates that the magnitude of the optical Kerr contribution to the diffracted signal depends strongly on the physical state of the liquid crystals. In addition, just as in conventional Kerr effect experiments, the birefringence experienced by the probe is a function of angle

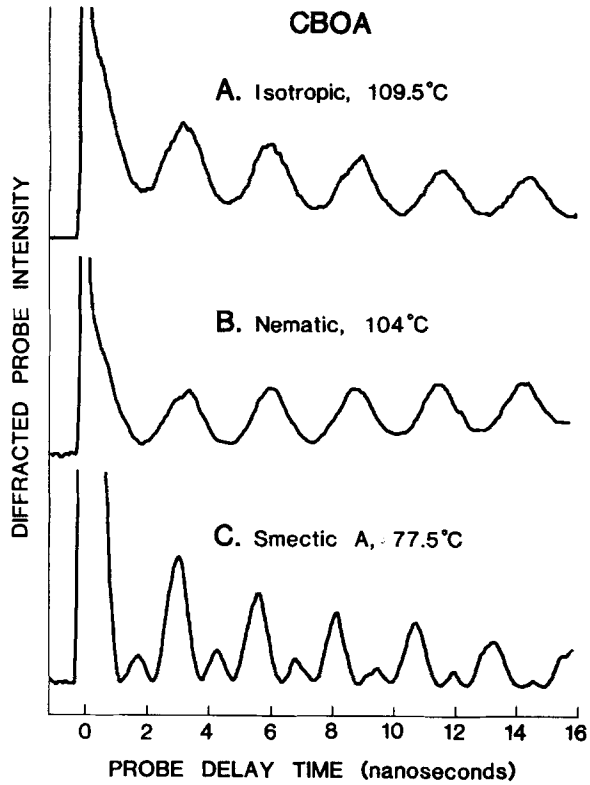

FIG. 5. Data taken under conditions identical to those in Fig. 4 but with parallel rather than perpendicular excitation pulse polarization. See text for the computation of acoustic parameters.

between the excitation and probe polarizations. This comes about because of the large anisotropy in the molecular susceptibility. Let us first consider the case of parallel excitation polarizations. We can define an (induced) order parameter Q by[6]

$$\delta n = n_{\parallel} - n_{\perp} = Q\Delta n, \tag{11}$$

where $n_{\parallel}$ and $n_{\perp}$ are the optical refractive indices parallel and perpendicular to the linearly polarized grating field, and Δn is the anisotropy in n when all the molecules are perfectly aligned in one direction. Since the unperturbed index is $n_0 = (n_{\parallel} + 2n_{\perp})/3$ we have $n_{\parallel} = n_0 + 2Q\Delta n/3$ and $n_{\perp} = n_0 - Q\Delta n/3$. Thus for a probe pulse traversing the grating with its polarization parallel to the excitation, the index oscillates between $n_{\parallel}$ in the intensity peaks and n_0 in the nulls, yielding a peak–null difference of $2Q\Delta n/3$. Similarly, for a perpendicularly polarized probe, the peak–null difference is $n_{\perp} - n_0 = -Q\Delta n/3$. With the diffraction efficiency proportional to $(n_{\text{peak}} - n_{\text{null}})^2$, we see that the signal is four times larger in the case of parallel probe polarization compared with perpendicular polarization. In addition, it is clear that the sign of the index change is reversed in the two cases. This corresponds to a change in sign of the cross term in Eq. (8), which means that if the experiment in Fig. 2A were repeated with the probe perpendicular to the excitation polarization, the positions of the bumps and dips in the signal would be reversed. We have verified this experimentally.

For the case of perpendicularly polarized excitation pulses, the situation is very different. We note in Fig. 3B that the linearly polarized components of the net field lie along

two (perpendicular) directions which are at 45° to the incident polarization. For small crossing angles θ, these resultant fields lie approximately in the plane of Fig. 3. These two directions, which we have labeled $\hat{e}_1$ and $\hat{e}_2$, are the natural basis vectors with which to describe the grating-induced birefringence (see Fig. 6). Consider a probe pulse polarized along either $\hat{e}_1$ or $\hat{e}_2$. In either case, the probe would encounter a periodic variation in the index of magnitude $|n_{\text{peak}} - n_{\text{null}}| = |n_{\parallel} - n_{\perp}| = Q\Delta n$, giving rise to identical diffraction efficiency for either polarization. Since any probe polarization can be written as a linear combination of components along $\hat{e}_1$ or $\hat{e}_2$, there is no probe polarization dependence to the diffraction intensity, in contrast to the factor of 4 for the grating in Fig. 3A.

In the discussion above we were careful to consider only the magnitude of the peak–null refractive index changes encountered by a probe of polarization $\hat{e}_1$ or $\hat{e}_2$, and we ignore the phases. We now show that the phases of the diffracted probe waves for the two polarizations must differ identically by π radians. This is precisely the operation performed on a wave front by a half-wave plate.

To see how this comes about, we observed that the orientational Kerr response in Fig. 3B results in alternating domains of partial orientation along $\hat{e}_1$ and $\hat{e}_2$. Due to the anisotropy of the refractive index, domains oriented along $\hat{e}_1$ have a higher refractive index for an $\hat{e}_1$-polarized probe and lower index for an $\hat{e}_2$-polarized probe, and vice versa. We can always describe an arbitrary probe polarization as a linear combination of components along $\hat{e}_1$ and $\hat{e}_2$. Figure 6 shows

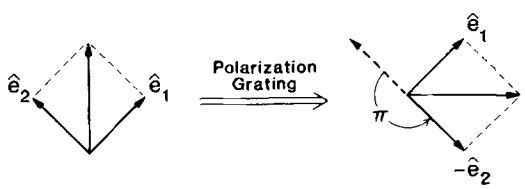

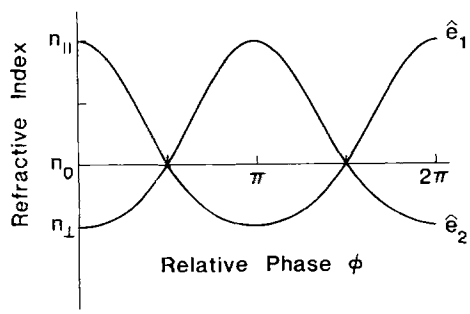

FIG. 6. The polarization grating of Fig. 3B acts as half-wave plate for the diffracted probe. Above: the vertical polarized incident probe is resolved into in-phase components along $\hat{e}_1$ and $\hat{e}_2$. The effect of the grating is to introduce a phase angle of π between the diffracted waves, which add vectorially to produce a horizontally polarized signal. Below: the refractive index variations experienced by the $\hat{e}_1$- and $\hat{e}_2$-polarized probe components as they traverse the grating. Note that these variations are exactly out-of-phase with each other. This causes the $\hat{e}_1$- and $\hat{e}_2$-polarized diffracted waves to have a phase difference of π.

the variations of the refractive indices for these components as a function of phase of the probe wave front. The zero of phase has been arbitrarily assigned to the point where the wave front encounters an $\hat{e}_1$-oriented domain. We see that the $n_{\hat{e}_1}$ curve is identical to the $n_{\hat{e}_2}$ curve except for a phase displacement of π radians. We consider the outgoing electric field to be a superposition of waves diffracted from the $\hat{e}_1$- and $\hat{e}_2$-polarized input waves. With an ordinary grating as in Fig. 3A, the phase relationship of the incoming waves is preserved in the outgoing waves, so the diffracted signal has the same polarization as the incident probe. Due to the phase displacement inherent in the grating in Fig. 3B, however, the phase of the outgoing $\hat{e}_2$ wave is shifted by π relative to the outgoing $\hat{e}_1$ wave, with the result that the signal polarization is rotated with respect to the incident probe polarization. As illustrated in Fig. 6, signal from a vertically polarized probe is horizontally polarized, and vice versa; $\hat{e}_1$- and $\hat{e}_2$-polarized probes have their polarization preserved, and signal from intermediate probe polarizations has a polarization which is a reflection of the incident polarization about the $\hat{e}_1$ or $\hat{e}_2$ axes.

The action of the grating in Fig. 3B, to alter the phase relationship between $\hat{e}_1$- and $\hat{e}_2$-polarized waves by exactly π in the outgoing diffracted wave, is precisely the action of a half-wave plate. However, the diffraction half-wave plate is less restricted than an ordinary transmission half-wave plate. For example, the effect is independent of the thickness of the grating, i.e., the number of fringes traversed by the probe. Also, it is independent of the wavelength of the probe, providing only that the probe is incident at the Bragg angle.

The transient polarization grating technique is applicable to systems other than those which display a Kerr effect. Any material which responds differently to different polarizations will display refractive index variations similar to those in Fig. 6. Moreover, use of perpendicular rather than parallel-polarized excitation pulses can simplify many transient grating experiments. The advantages of this geometry for the case of amplitude gratings has been discussed by von Jena and Lessing.[21] Of particular importance is the rotation of the signal polarization, which permits the use of a polarizer to separate signal from the scattered light background.

CONCLUDING REMARKS

In the foregoing we have discussed how transient grating techniques can be used to investigate the rotational dynamics and mechanical properties of liquid crystal films. Using 100 ps excitation pulses, we have observed a fast nonexponential component to the Kerr relaxation not resolved by previous workers who used $\sim$20 ns pulses. This relaxation is associated with a distribution of times ranging from $\sim 10^{-10}$–10^{-9} s. We have interpreted this result in terms of angular diffusion of the molecular long axes in spontaneously formed "pockets" whose size and number depend on the temperature and phase of liquid crystals. In order to characterize this process more fully, we intend to repeat these experiments using excitation and probe pulses of 1 ps or less.

The advantages of transient grating methods in ultra-

sonic experiments have been enumerated previously.[4,5] These include the frequency tunability, the capacity to measure very high attenuations accurately, and, recently, the coherent generation of shear waves.[10] It would especially be of interest to extend these experiments to the 10^7–10^8 Hz range where the acoustic waves can couple effectively to the liquid crystal order parameter.[18] Under these conditions, the acoustic attenuation displays an anomalous dispersion near the phase transition which provides information on critical relaxation processes. One important application of this technique will be the study of mechanical properties of planar phospholipid bilayers in various states of hydration and containing biologically interesting ingredients. Large monodomain multibilayer arrays can be prepared with high optical quality and at thicknesses comparable to those used in the present work.[22] The mechanical properties of such samples are difficult to measure by more conventional methods,[23] and are currently under investigation in our laboratory.

ACKNOWLEDGMENTS

This work was supported by a grant from the National Institute of Health (No. GM32205). Equipment used in the experiments was provided by the National Science Foundation (Grant No. DMR 79-20380).

[1]M. D. Fayer, Annu. Rev. Phys. Chem. **33**, 63 (1982).
[2]R. J. Dwayne Miller, M. Pierre, and M. D. Fayer, J. Chem. Phys. **78**, 5138 (1983).
[3]R. S. Moog, M. D. Ediger, S. G. Boxer, and M. D. Fayer, J. Phys. Chem. **86**, 4694 (1982).
[4]K. A. Nelson and M. D. Fayer, J. Chem. Phys. **72**, 5202 (1980).
[5]R. J. Dwayne Miller, R. Casalegno, K. A. Nelson, and M. D. Fayer, Chem. Phys. **72**, 371 (1982).
[6]G. K. L. Wong and Y. R. Shen, Phys. Rev. A **10**, 1277 (1974).
[7]H. J. Coles and B. R. Jennings, Mol. Phys. **36**, 50 (1978).
[8]K. Sala and M. C. Richardson, Phys. Rev. A **12**, 1036 (1976).
[9]K. Miyano and J. B. Ketterson, in *Physical Acoustics*, edited by P. Mason and R. N. Thurston (Academic, New York, 1979), Vol. XIV, p. 93.
[10]Keith A. Nelson, J. Appl. Phys. **53**, 6060 (1982).
[11]D. R. Lutz, Ph.D. thesis, Stanford University, 1981.
[12]G. Eyring and M. D. Fayer, Chem. Phys. Lett. **98**, 428 (1983).
[13]E. P. Ippen and C. V. Shank, Appl. Phys. Lett. **26**, 92 (1975).
[14]M. Doi and S. F. Edwards, J. Chem. Soc. Faraday Trans. 2, **74**, 560 (1978).
[15]K. M. Zero and R. Pecora, Macromolecules **15**, 87 (1982).
[16]G. Williams, J. Pol. Sci. **21**, 2037 (1983).
[17]J. A. Janik, M. Godlewska, T. Grochulski, A. Kocot, E. Sciesinska, J. Sciesinski, and W. Witco, Mol. Cryst. Liq. Cryst. **98**, 67 (1983).
[18]S. Candau and S. V. Letcher, Adv. Liq. Cryst. **3**, 167 (1978).
[19]C. Druon and J. M. Wacrenier, Mol. Cryst. Liq. Cryst. **98**, 201 (1983).
[20]S. D. Durbin, S. M. Arakelian, M. M. Cheung, and Y. R. Shen, J. Phys. Colloq. (Paris) C **2**, 161 (1983).
[21]A. von Jena and H. E. Lessing, Opt. Quantum Electron. **11**, 419 (1979).
[22]L. Powers and P. S. Pershan, Biophys. J. **20**, 137 (1977).
[23]J.-P. LePesant, L. Powers, and P. S. Pershan, Proc. Natl. Acad. Sci. U.S.A. **75**, 1792 (1978).